Long-haul transmission of 16×52.5 Gbits/s polarization-division-multiplexed OFDM enabled by MIMO processing (Invited)

Sander L. Jansen,[1,*] Itsuro Morita,[1] Tim C. W. Schenk,[2] and Hideaki Tanaka[1]

[1]*KDDI R&D Research Laboratories, 2-1-15 Ohara, Fujimino, Saitama, 356-8502, Japan*
[2]*Philips Research, Eindhoven, the Netherlands*
**Corresponding author: SL-Jansen@kddilabs.jp*

Received November 1, 2007; accepted December 17, 2007;
published January 18, 2008 (Doc. ID 89311)

We discuss the realization and performance of polarization-division-multiplexed orthogonal frequency division multiplexing (PDM-OFDM) for long-haul transmission systems. Polarization demultiplexing of the PDM signal at the receiver is realized by employing a multiple-input multiple-output (MIMO) detector. Using a recirculating loop a long-haul transmission experiment is reported of 52.5 Gbits/s PDM-OFDM (40 Gbits/s after coding) over 4160 km of standard single-mode fiber (SSMF). In this transmission experiment, 16 wavelength-division-multiplexed (WDM) channels are transmitted at 50 GHz channel spacing, and we show that MIMO processing in the receiver enables both polarization demultiplexing and a large PMD tolerance.

OCIS codes: 060.2330, 060.4080.

1. Introduction

Polarization division multiplexing (PDM) is a very effective method for doubling the spectral efficiency of a transmission system [1,2]. However, it has been shown that direct-detected PDM has a reduced tolerance to polarization mode dispersion (PMD), because the polarization demultiplexing introduces cross talk between the polarization tributaries [3]. An elegant way to overcome this PMD sensitivity is by using polarization diverse coherent detection with digital equalization instead of direct detection. In [4] it has been shown that such a system can effectively be described as a polarization multiple-input multiple-output (MIMO) system in which any space–time coding algorithm can be applied. This has enabled the demonstration of various single-carrier MIMO experiments with bit rates up to 111 Gbits/s and a superior tolerance toward chromatic dispersion and PMD [5].

Orthogonal frequency division multiplexing (OFDM) presents an alternative to digital coherent systems that inherently offers a virtually unlimited chromatic dispersion [6] and PMD [7] tolerance and is furthermore easier scalable to higher level modulation formats [8–10]. It has therefore received considerable interest in the fiber-optic community [5–12]. Recently, we reported the first, to the best of our knowledge, realization of PDM-OFDM transmission by MIMO processing at the receiver [13]. In this experiment 16×52.5 Gbits/s (40 Gbits/s after coding) PDM-OFDM transmission over 4160 km of standard single-mode fiber (SSMF) was realized with 50 GHz WDM channel spacing.

In this paper, we give a detailed explanation of MIMO processing for PDM-OFDM transmission systems and elaborate on the results obtained in [13]. The paper is structured as follows. In Section 2 the concept of MIMO processing for PDM systems is explained. Subsequently, a detailed description of the experimental setup for the long-haul PDM-OFDM experiment is described in Section 3. Section 4 discusses the obtained experimental results and a brief discussion is presented in Section 5. In Section 6 we draw the conclusions.

2. Polarization-Division-Multiplexing Receiver With MIMO Processing

The concept of a PDM transmission system with coherent optical detection and MIMO processing at the receiver is shown in Fig. 1. At the transmitter two baseband signals, generated by transmitters 1 and 2, are modulated onto an optical carrier and multiplexed onto orthogonal polarizations by a polarization beam splitter. For an optical OFDM system, modulation can be either done with an electrical inphase-quadrature (IQ) mixer in combination with a single-ended Mach–Zehnder modulator (MZM) [6], or with a complex IQ modulator as optical IQ mixer [9,10]. At the receiver first the received signal is split into two random polarizations. The two detected signals consist of an arbitrary mix of each transmitted signal. To preserve the phase information of the optical signal, two coherent optical detectors (CODs) are used for conversion from the optical to the electrical domain. MIMO processing is then applied to derotate the polarization and separate the two received signals. After MIMO processing, the two derotated signals are fed to the baseband receivers.

In Fig. 1 a PDM system with MIMO processing is depicted for a system with coherent detection at the receiver. Note that OFDM has been proposed as well for direct-detected systems [8,11,12] and in such systems MIMO processing can be implemented as well. However, for direct-detected optical (DDO) OFDM an additional polarization control is required at the receiver to equally split the power of the optical carrier over the two optical front ends in order to realize a polarization diverse receiver [14]. Even though in a PDM-DDO-OFDM system polarization control is required, this system is unlike direct-detected PDM systems tolerant toward PMD because of the MIMO processing at the receiver.

2.A. PDM-OFDM

Figure 2 illustrates the block diagram of a PDM-OFDM transmitter and receiver. For simplicity, a perfectly synchronized system is assumed in this illustration, meaning that the carrier frequency offset (CFO) [15] and local oscillator phase noise [6] is compensated for. The OFDM transmitter consists effectively of two conventional OFDM transmitters. The notation vectors shown in Fig. 2 consist of two elements, one for each transmitter, defined for data stream **b** as

$$\mathbf{b} = \begin{pmatrix} b_1 \\ b_2 \end{pmatrix}, \tag{1}$$

where the index denotes the number of the transmitter. Vectors and matrices are denoted by bold lower and upper case symbols, respectively. The binary data stream **b** is converted from serial to parallel and symbol mapping is applied. Periodically, training symbols are then inserted resulting in the complex signal vector **s**. Subsequently, the signal is modulated onto orthogonal carriers by taking the inverse fast Fourier transform (IFFT). After the IFFT, cyclic prefix is added to mitigate impairments caused by, for instance, chromatic dispersion or PMD, yielding the OFDM baseband vector **u**. The baseband signals of both transmitters are then converted to analog signals using digital-to-analog converters (DACs) and fed to the optical front end (shown in Fig. 1). At the receiver, the outputs of the optical front end are first digitalized using analog-to-digital converters (ADCs), yielding vector **y**. After the ADCs, symbol synchronization is applied as described in [15,16]. Both transmitters operate at the same symbol rate, so the symbol timing needs only to be recovered once. The OFDM signal is converted back to the frequency domain by taking the fast fourier transform (FFT), yielding signal vector **x**. After the FFT, the training symbols are removed from

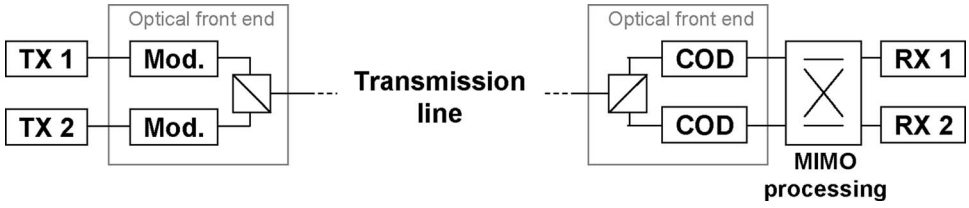

Fig. 1. Concept of PDM enabled by MIMO processing at the receiver, with TX = baseband transmitter, Mod. = Modulator, COD = coherent optical detector, and RX = baseband receiver.

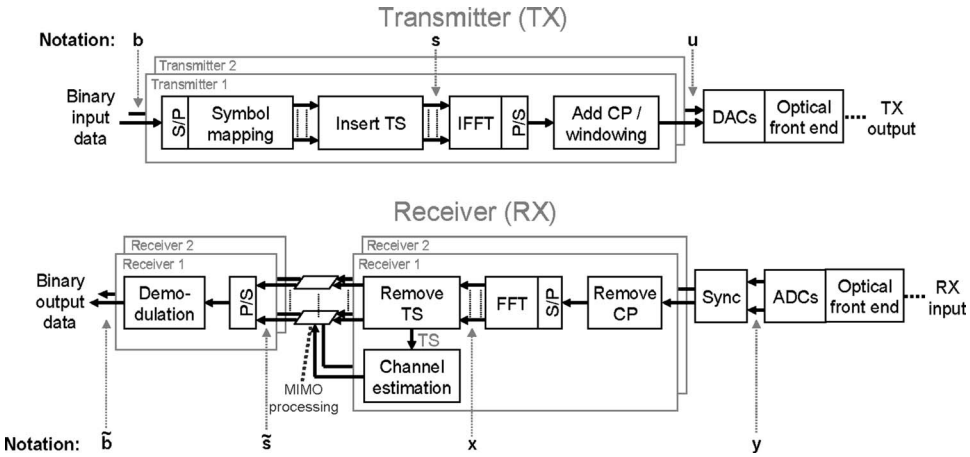

Fig. 2. Block diagram of a PDM-OFDM transmitter and receiver, with S/P=serial to parallel, P/S=parallel to serial, CP=cyclic prefix, TS=training symbol, DAC=digital-to-analog converter, ADC=analog-to-digital converter, CFO corr.=carrier frequency offset correction, and Sync=OFDM symbol synchronization.

the payload and used for channel estimation. Subsequently, MIMO processing per subcarrier is applied to derotate the polarization of the received symbols, yielding estimate vector $\tilde{\mathbf{s}}$. Finally, these symbols are demodulated (or demapped) resulting in the estimate vector of the transmitted data $\tilde{\mathbf{b}}$. Numerous system parameters are critical for the design of an OFDM system and in [6] some of the most important parameters and trade-offs for OFDM-based fiber-optic transmission systems are discussed. In this section the enabling techniques for MIMO processing will be reviewed: MIMO processing and channel estimation.

2.B. MIMO Processing

In a single-carrier PDM system, a butterfly structure of complex valued, multitap adaptive filters has proven to be an effective equalizer for MIMO processing [5]. This equalizer can theoretically be applied to multicarrier systems such as OFDM as well, but would result in an immense computational complexity as a separate adaptive filter has to be applied for each individual OFDM subcarrier. It has been shown that for a multicarrier system, the computational complexity of a MIMO detector can greatly be reduced by using knowledge about the channel at the receiver [17]. Such a MIMO detector will be discussed in this section.

Assuming a perfectly synchronized system, the received signal before MIMO processing $\mathbf{x}(k)$ of the kth subcarrier can be expressed as

$$\mathbf{x}(k) = \mathbf{H}(k)\mathbf{s}(k) + \mathbf{n}(k), \tag{2}$$

where

$$\mathbf{H}(k) = \begin{pmatrix} h_{11} & h_{12} \\ h_{21} & h_{22} \end{pmatrix}, \tag{3}$$

represents the 2×2 channel matrix (Jones matrix) and vector $\mathbf{n}(k)$ represents the frequency-domain noise within subcarrier k for the two received polarizations. The most straightforward MIMO detector employs a zero forcing (ZF) algorithm. Basically, ZF-MIMO detection is realized by multiplying the received signals $\mathbf{x}$ with the pseudoinverse of the estimated channel matrix to find an estimate of the transmitted vector [18]. For subcarrier k, let $\tilde{\mathbf{H}}(k)$ be the estimation of channel matrix $\mathbf{H}(k)$; the estimate of the transmitted stream after ZF processing $\tilde{\mathbf{s}}(k)$ can then be described by

$$\tilde{\mathbf{s}}(k) = \tilde{\mathbf{H}}^{+}(k)\mathbf{x}(k), \tag{4}$$

where superscript + denotes the pseudoinverse operation, defined for a matrix $\mathbf{A}$ as

$$\mathbf{A}^{+} = (\mathbf{A}^{H}\mathbf{A})^{-1}\mathbf{A}^{H}. \tag{5}$$

Here H and -1 denote the conjugate transpose and matrix inverse, respectively. Assuming perfect channel estimation, i.e., $\tilde{\mathbf{H}}^{+}(k) = \mathbf{H}^{+}(k)$, Eq. (4) can be written as

$$\tilde{\mathbf{s}}(k) = \mathbf{s}(k) + \mathbf{H}^{+}(k)\mathbf{n}(k). \tag{6}$$

From Eq. (6) we see that even with perfect channel estimation an error term will occur due to the noise added by optical amplifiers and other noise sources. More advanced MIMO detectors can be employed to improve the performance in MIMO detection, such as parallel interference detection [19] and maximum-likelihood detection (MLD) [20,21]. However, this performance improvement comes at the cost of a significant increase in computational complexity.

2.C. MIMO OFDM Channel Estimation

For MIMO processing to work, an estimation of the MIMO channel is required in the receiver. A commonly used method to enable channel estimation is by periodically inserting a piece of known data, i.e., a training symbol, in the symbol stream at the transmitter. At the receiver, channel estimation can then be realized by comparing the received symbol per OFDM subcarrier with the transmitted training symbol. As shown in Fig. 2, channel estimation is performed in the frequency domain, e.g., after the FFT operation at the receiver. For a MIMO system, it is essential that the training symbols of the transmitters are orthogonal so that they can be uniquely identified at the receiver [22]. To, at the same time, characterize the frequency selective behavior, e.g., caused by chromatic dispersion, the used training symbols should also be shift orthogonal. To achieve this, several training symbol structures have been proposed in the literature. In this section only the time-multiplexed training symbols, illustrated in Fig. 3, will be discussed. Each training period consists of two OFDM training symbols $s_{1,t1}$ and $s_{2,t2}$ that are transmitted by transmitter 1 and transmitter 2, respectively. Indices t1 and t2 refer to the time-slot number within the training period. In the time-multiplexed symbol configuration, orthogonality between the two transmitters is realized by sending the OFDM training symbols one after the other.

The received signals on the kth subcarrier during the training period can now, using Eq. (2), be written as the 2×2 matrix

$$\begin{aligned}\mathbf{X}_t(k) &= [\mathbf{x}_{t1}(k)\mathbf{x}_{t2}(k)] = \mathbf{H}(k)\mathbf{S}_t(k) + \mathbf{N}_t(k) = \mathbf{H}(k)[\mathbf{s}_{t1}(k)\mathbf{s}_{t2}(k)] + [\mathbf{n}_{t1}(k)\mathbf{n}_{t2}(k)] \\ &= \mathbf{H}(k)\begin{pmatrix} s_{1,t1}(k) & 0 \\ 0 & s_{2,t2}(k) \end{pmatrix} + [\mathbf{n}_{t1}(k)\mathbf{n}_{t2}(k)],\end{aligned} \tag{7}$$

where $\mathbf{x}_{t1}(k)$ denotes the 2×1 received signal vector for the kth subcarrier during time slot t1. The notation for the noise and transmitted signal vectors is the same. Consequently, an estimate can be derived from the received signal matrix using different estimation algorithms, such as least-squares estimation (LSE) and minimum mean-squared error estimation (MMSE). Here we will review the former, for which an estimate of the MIMO channel matrix is found as

$$\tilde{\mathbf{H}}(k) = \mathbf{X}_t(k)\mathbf{S}_t^{+}(k) = \mathbf{H}(k) + \mathbf{N}_t(k)\mathbf{S}_t^{+}(k). \tag{8}$$

An effective method to reduce the impact of the error caused by the noise term, i.e., the last term in Eq. (8), is to apply averaging with a moving average algorithm over time and/or frequency. For time averaging, typical average window lengths are between 5 and 50, depending on the system configuration. Furthermore, in order to

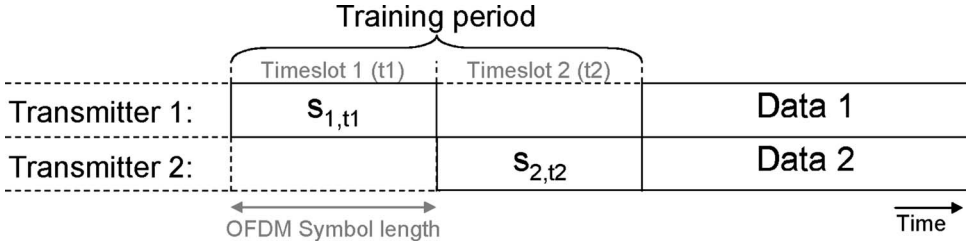

Fig. 3. Time-multiplexed training symbols for MIMO channel estimation.

minimize the influence of nonlinearities on channel equalization, a training symbol is usually constructed such that it exhibits a low peak-to-average power ratio (PAPR).

3. Experimental Setup

The performance of 52.5 Gbits/s PDM-OFDM was evaluated in a WDM environment on a long-haul transmission link. The experimental setup of the transmitter is shown in Fig. 4 and the inset of this figure illustrates the electrical OFDM channel allocation. The 52.5 Gbits/s OFDM signal consists of two polarization- subcarrier-multiplexed OFDM bands, so in total four 13.1 Gbits/s tributaries. Two Tektronix AWG7102 arbitrary waveform generators (AWG) are used to produce a 13.1 Gbits/s OFDM baseband signal each. The waveforms produced by the AWG have been calculated offline and are outputted continuously. The OFDM signal bandwidth is 10 GHz, which is split up in 256 subchannels, of which 168 carry data. Quadrature phase-shift keying (QPSK) modulation is used for symbol mapping and the cyclic prefix length is 40 samples (4 ns) per OFDM symbol. As a result, the OFDM symbol length is 29.6 ns and the OFDM symbol rate 33.8 MHz. Both OFDM baseband signals are upconverted to two intermediate frequencies (IF) by electrical IQ mixers, namely, 11.5 and 18.7 GHz. After upconversion, passive 6 dB power combiners are used to combine the upconverted signals so that the configuration shown in the inset of Fig. 4 is realized. More details about the OFDM baseband generation and IQ mixing can be found in [6].

For this WDM experiment, 16 external cavity lasers (ECLs) with 100 kHz linewidth are aligned on a 50 GHz ITU grid between 1551.3 and 1557.4 nm. Two parallel modulator structures are used in this setup for separate modulation of the even and odd channels. Each modulator structure consists of two single-ended MZM modulators to modulate each polarization independently. Subsequently, the two PDM signals are combined using a polarization beam splitter and the even and odd WDM channels are combined with a 50 GHz interleaver. As illustrated in Fig. 4, the interleaver is aligned such that the image band of the OFDM signal is rejected.

The experimental setup of the recirculating loop and the receiver is shown in Fig. 5. The recirculating loop consists of four spans of 80 km SSMF without optical dispersion compensation. After every span, amplification is provided by a Raman–erbium-doped fiber amplifier (EDFA) structure with an average ON–OFF Raman gain of ~6 dB. A dynamic gain equalizer (DGE) is used for power equalization and a loop-synchronous polarization scrambler (LSPS) is employed to reduce loop-induced polarization effects. A polarization maintaining fiber with a differential group delay (DGD) of 86 ps is added to the recirculating loop. After 13 round trips this emulates a ~300 ps average PMD.

At the receiver, the signal is split in two random polarizations and detected with a polarization-diversity heterodyne receiver. An ECL with ~100 kHz linewidth is used as free running local oscillator (LO). Subsequently, a real-time digital storage oscilloscope (DSO) is used to sample the two outputs of the heterodyne receiver. The bandwidth of the ADCs in the DSO is 16 GHz, the sampling frequency is 50 GHz and the effective vertical resolution is approximately 4.5 bits. After detection, the data is post-processed off-line. A bandpass filter (BPF) is first used to select one of the OFDM bands. To compensate for the phase noise of the local oscillator, RF-aided phase noise

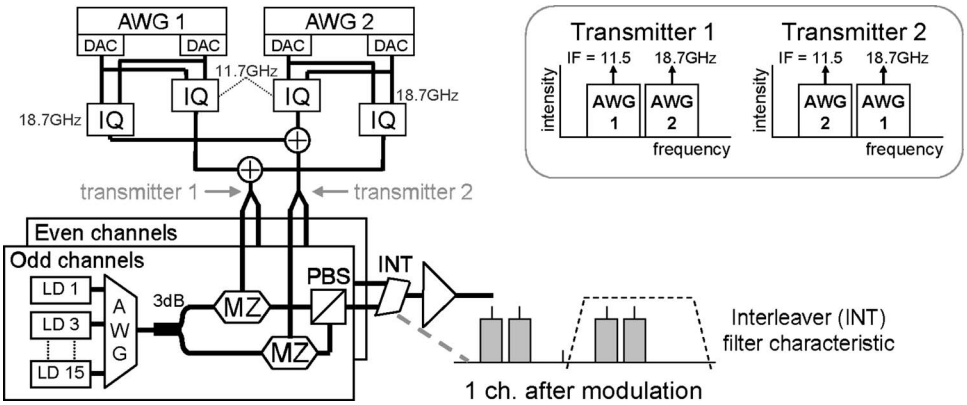

Fig. 4. Experimental setup of the 16×52.5 Gbits/s PDM-OFDM transmitter.

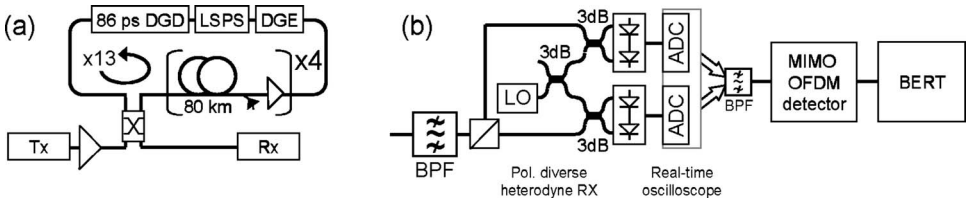

Fig. 5. Experimental setup of (a) the recirculating loop and (b) the polarization diverse, heterodyne receiver.

compensation is implemented (for the implementation, see [6]). Subsequently, the signal is fed to the MIMO OFDM detector as shown in Fig. 2. To mitigate the influence of amplified spontaneous emission (ASE) noise on the channel estimation, a moving average of 44 training symbols was used for MIMO processing at the receiver. After the MIMO detector, the bit error rate (BER) is estimated. For all reported BERs $10 \times (1.3 \times 10^6)$ bits have been evaluated, each with different polarization state settings in the LSPS. The bit rate before coding is 52.5 Gbits/s, from which 6% is used for training symbols and 15.6% for the cyclic prefix. Taking an additional 7% for forward error correction (FEC) coding into account, this results in a net 40 Gbits/s bit rate.

4. Experimental Results

Figure 6 shows the measured back-to-back sensitivities for 26.3 Gbits/s (single polarization) and 52.5 Gbits/s (PDM). Additionally, the simulated sensitivity for 26.3 Gbits/s (single polarization) is shown as well. The required optical signal-to-noise ratio (OSNR) for a BER of 1×10^{-3} is 8.4 and 11.3 dB/0.1 nm for 26.3 and 52.5 Gbits/s, respectively. The 26.3 Gbits/s sensitivity is more than 3.5 dB better than that reported in our previous experiment [6]. This improvement is mainly realized by reducing the nonlinearities in the electrical amplifiers. Compared to the simulated sensitivity of 26.3 Gbits/s a 1.4 dB penalty at a BER of 1×10^{-3} is present in the experiment. For lower BER values an increase in performance penalty between the simulated and experimental curve is observed. This penalty increase is probably caused by the fact that at lower BER values the residual CFO and phase noise after compensation start influencing the system performance [16,23].

Between the measured 26.3 Gbits/s single polarization and 52.5 Gbits/s PDM curves a 3 dB OSNR difference is measured and it can thus be concluded that the penalty caused by ZF-based MIMO detection is negligible. The BER curves of the four individual 13.1 Gbits/s tributaries of the 52.5 Gbits/s PDM-OFDM signal are shown in gray in Fig. 6. Between these tributaries, a ~1 dB difference in OSNR is measured resulting from small electrical and optical power imbalances at the transmitter.

To assess the influence of interchannel cross-phase modulation (XPM), two transmission experiments are conducted; one where the channel under investigation (located at 1553.7 nm) is surrounded by 50 GHz spaced neighboring channels and one where the channel spacing is increased to 200 GHz. Figure 7(a) shows the measured common phase rotation (CPR) of all the subcarriers in one OFDM symbol after 3200 km transmission as a function of the fiber launch power. In the linear regime (low fiber launch powers) a low CPR is observed for both 50 and 200 GHz channel

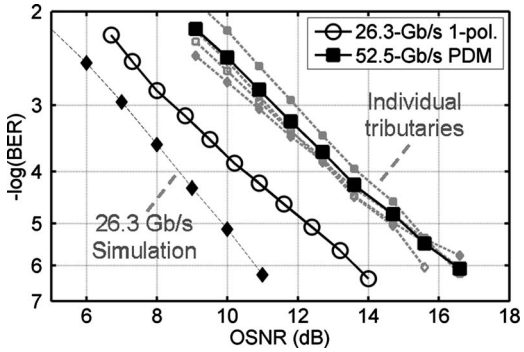

Fig. 6. BER as a function of the OSNR for 26.3 Gbits/s OFDM (single polarization) and 52.5 Gbits/s PDM-OFDM.

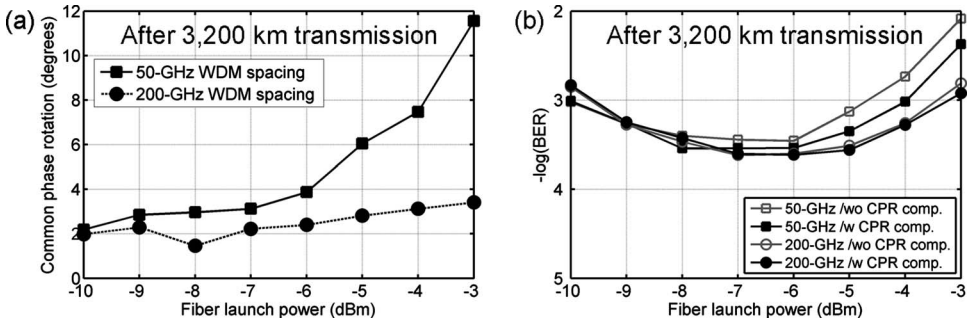

Fig. 7. (a) BER as a function of the fiber launch power per channel after 3200 km transmission. (b) Common phase rotation as a function of the fiber launch power per channel after 3200 km transmission.

spacing. However, for high launch powers, a steep increase in CPR is observed for the 50 GHz spaced configuration due to interchannel XPM, whereas at 200 GHz channel spacing the CPR is nearly unaffected.

The BER as a function of the fiber launch power after 3200 km transmission [Fig. 7(b)] shows similar results. For this experiment a simple CPR compensator was implemented by multiplying the received constellation with the inverse of the CPR [24]. At 200 GHz channel spacing, interchannel nonlinear impairments are negligible and as a result the BER performance with and without CPR compensation is practically the same. At 50 GHz channel spacing an improvement in BER is observed for high input powers when CPR compensation is employed. This indicates that interchannel XPM induced CPR somewhat degrades the transmission performance and as such reduces the optimum launch power by ~1 dB.

In the nonlinear regime only a small difference in BER performance is observed between 50 and 200 GHz channel spacing when CPR is compensated for. Thus, it can be concluded that in such a system intrachannel four-wave mixing (IFWM) is dominant over interchannel XPM, even at 50 GHz WDM channel spacing [24,25].

Most phase noise compensation schemes proposed for coherent optical (CO) OFDM transmission systems use pilots to compensate for laser phase noise at the receiver [6,7]. These pilots are impaired by IFWM components just like the OFDM data subcarriers and thereby the accuracy of phase noise compensation at the receiver is reduced. In this transmission experiment RF-aided phase noise compensation is used to compensate for the laser phase noise. This technique employs one single RF pilot that is inserted in the middle of the OFDM spectrum. The RF-aided pilot after 3200 km transmission is shown in Fig. 8 for fiber launch powers of −10 and −3 dBm. At high fiber launch powers, the IFWM products that fall in the RF-pilot window can clearly be seen. The IFWM products within the RF pilot can be reduced by increasing the guard band between the RF pilot and the OFDM band through the insertion of unmodulated subcarriers [26]. However, the addition of unmodulated channels in the middle of the OFDM band will slightly increase the overhead.

Figure 9(a) shows the performance of the 16 WDM channels after 4160 km transmission. The fiber launch power in this experiment was set to −7 dBm, resulting in an average OSNR after transmission of 14.9 dB. Although a difference in BER perfor-

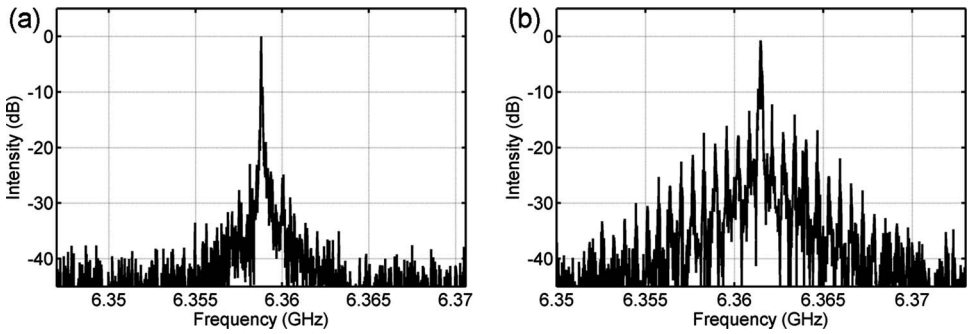

Fig. 8. (a) Electrical spectrum of the RF-aided pilot after 3200 km transmission at 1.25 kHz resolution bandwidth. (a) −10 dBm fiber launch power, (b) −3 dBm fiber launch power.

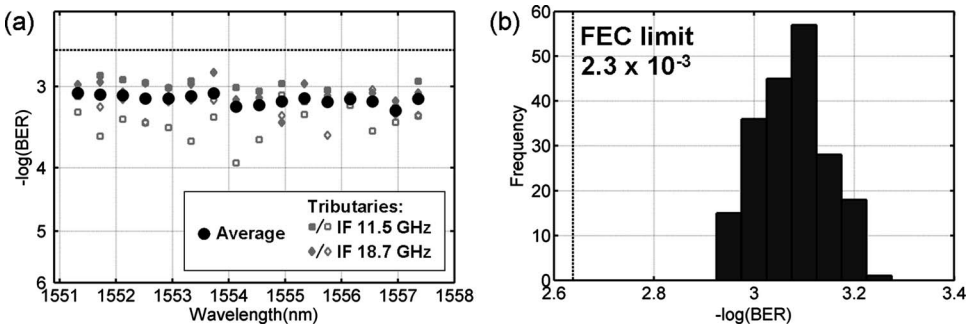

Fig. 9. (a) BER per channel after 4160 km transmission, (b) BER histogram of 200 $\times(1.3\times10^{6})$ recordings.

mance of more than a factor of 10 is present between the four individual 13.1 Gbits/s tributaries, the average BER per channel shows little variation and varies only between 5.4×10^{-4} and 8.5×10^{-4}. This is well below the threshold of a concatenated FEC code with 7% overhead (2.3×10^{-3} corrected to 1×10^{-12}).

To observe the long-term behavior of the transmission link, the channel with the worst performance (located at 1553.7 nm) was monitored over 200 recordings of 1.3×10^{6} bits (260×10^{6} bits total). The BER histogram is shown in Fig. 9(b), which shows a BER variation between 5.9×10^{-4} and 1.2×10^{-3}. The average BER is 8.5×10^{-4} for this channel. Without the DGD element in the transmission line only a slight improvement in average BER (7.5×10^{-4}) is observed. Hence, we conclude that even ~300 ps of average PMD results in a negligible penalty.

5. Discussion

A disadvantage of OFDM transmission system is the increased overhead resulting from training symbols, cyclic prefix, and, in some cases, pilot subcarriers used for phase noise and residual CFO correction. In the experiment discussed in Sections 3 and 4, 40 Gbits/s transmission is realized with a total 52.5 Gbits/s nominal data rate (data rate before coding), hence a total overhead of 31.3%. However, in particular the overhead caused by the cyclic prefix was large (15.6%). The cyclic prefix overhead can potentially be reduced by increasing the FFT size, since this also increases the OFDM symbol length. For example, when the FFT size is increased from 256 to 1024, the cyclic prefix overhead would be reduced from 15.6% to a mere 4.9%. It is noted, however, that the FFT size cannot be increased unlimited, since a larger FFT requires higher processing complexity and since a higher number of subcarriers result in an increased sensitivity to laser phase noise. The overhead of training symbols can be reduced by using either shorter training symbols or by increasing the training symbol spacing. Furthermore, for MIMO-OFDM training symbols, the number of OFDM symbols per training period can be reduced by using more advanced training symbol structures, such as the subcarrier-multiplexed or the subcarrier-orthogonal configuration [16]. With such techniques, the total overhead for OFDM modulation can realistically be reduced to ~15% (including FEC), slightly depending on the system configuration. Hence, OFDM modulation will normally have approximately double the overhead of what is required for single-carrier modulation formats (7%), but at the advantage of creating a truly transparent modulation format that does not require *a priori* knowledge about the transmission link.

6. Conclusion

In this paper MIMO processing for polarization demultiplexing is discussed for polarization-division-multiplexed OFDM (PDM-OFDM) transmission systems. Using time-multiplexed training symbols and zero-forcing MIMO processing we reported the realization 52.5 Gbits/s PDM-OFDM. For MIMO processing itself a negligible OSNR penalty was observed. In a 50 GHz spaced WDM environment, successful transmission is demonstrated of 16×52.5 Gbits/s over 4160 km SSMF in the presence of large amounts of PMD.

Acknowledgments

The authors thank D. van den Borne from the Eindhoven University of Technology, the Netherlands, and Dr. S. Randel from the Siemens A.G. in Munich for many fruitful discussions. Furthermore, the authors thank S. Akiba and M. Suzuki from KDDI R&D Laboratories for their support. This work was partly supported by the National Institute of Information and Communications Technology of Japan.

References

1. A. H. Gnauck, G. Charlet, P. Tran, P. J. Winzer, C. R. Doerr, J. C. Centanni, E. C. Burrows, T. Kawanishi, T. Sakamoto, and K. Higuma, "25.6-Tb/s C+L-band transmission of polarization-multiplexed RZ-DQPSK signals," in *Proceedings of the Optical Fiber Communication Conference* (IEEE, 2007), paper PDP 19.
2. H. Masuda, A. Sano, T. Kobayashi, E. Yoshida, Y. Miyamoto, Y. Hibino, K. Hagimoto, T. Yamada, T. Furuta, and H. Fukuyama, "20.4-Tb/s (204×111 Gb/s) transmission over 240 km using bandwidth-maximized hybrid Raman/EDFAs," in *Proceedings of the Optical Fiber Communication Conference* (IEEE, 2007), paper PDP 20.
3. D. v. d. Borne, N. E. Hecker-Denschlag, G. D. Khoe, and H. d. Waardt, "PMD-induced transmission penalties in polarization-multiplexed transmission," J. Lightwave Technol. **23**, 4004–4015 (2005).
4. Y. Han and G. Li, "Coherent optical communication using polarization multiple-input–multiple-output," Opt. Express **13**, 7527–7534 (2005).
5. C. R. S. Fludger, T. Duthel, D. van den Borne, C. Schulien, E.-D. Schmidt, T. Wuth, E. de Man, G. D. Khoe, and H. de Waardt, "10×111 Gbit/s, 50 GHz spaced, POLMUX-RZ-DQPSK transmission over 2375 km employing coherent equalisation," in *Proceedings of the Optical Fiber Communication Conference* (IEEE, 2007), paper PDP 22.
6. S. L. Jansen, I. Morita, T. C. W. Schenk, N. Takeda, and H. Tanaka, "Coherent optical 25.8-Gb/s OFDM transmission over 4,160-km SSMF," J. Lightwave Technol. **26** (to be published).
7. W. Shieh, X. Yi, Y. Ma, and Y. Tang, "Theoretical and experimental study on PMD-supported transmission using polarization diversity in coherent optical OFDM systems," Opt. Express **15**, 9936–9947 (2007).
8. B. J. C. Schmidt, A. J. Lowery, and J. Armstrong, "Experimental demonstrations of 20 Gbit/s direct-detection optical OFDM and 12 Gbit/s with a colorless transmitter," in *Proceedings of the Optical Fiber Communication Conference* (IEEE, 2007), paper PDP 18.
9. X. Yi, W. Shieh, and Y. Ma, "Phase noise on coherent optical OFDM systems with 16-QAM and 64-QAM beyond 10 Gb/s," presented at the European Conference on Optical Communication, Berlin, Germany, 16–20 September 2007, paper Tu. 2.5.3.
10. S. L. Jansen, I. Morita, and H. Tanaka, "Experimental demonstration of 23.6-Gb/s OFDM with a colorless transmitter," in *Proceedings of the Optoelectronics and Communications Conference* (IEICE, 2007), paper PD1-5.
11. S. C. J. Lee, F. Breyer, S. Randel, M. Schuster, J. Zeng, F. Huijskens, H. P. A. van den Boom, A. M. J. Koonen, and N. Hanik, "24-Gb/s transmission over 730 m of multimode fiber by direct modulation of an 850-nm VCSEL using discrete multi-tone modulation," in *Proceedings of the Optical Fiber Communication Conference* (IEEE, 2007), paper PDP 6.
12. I. B. Djordjevic and B. Vasic, "Orthogonal frequency division multiplexing for high-speed optical transmission," Opt. Express **14**, 3767–3775 (2006).
13. S. L. Jansen, I. Morita, and H. Tanaka, "16×52.5-Gb/s, 50-GHz spaced, POLMUX-CO-OFDM transmission over 4,160 km of SSMF enabled by MIMO processing," presented at the European Conference on Optical Communication, Berlin, Germany, 16–20 September 2007, paper PD1.3.
14. M. Mayrock and H. Haunstein, "PMD tolerant direct-detection optical OFDM system" presented at the European Conference on Optical Communication, Berlin, Germany, 16–20 September 2007, paper Tu 5.2.5.
15. T. M. Schmidl and D. C. Cox, "Robust frequency and timing synchronization for OFDM," IEEE Trans. Commun. **45**, 1613–1621 (1997).
16. T. C. W. Schenk, *RF Imperfections in High-Rate Wireless Systems* (Springer, 2008).
17. A. van Zelst and T. C. W. Schenk, "Implementation of a MIMO OFDM-based wireless LAN system," IEEE Trans. Signal Process. **52**, 483–494 (2004).
18. J. H. Winters, "On the capacity of radio communication systems with diversity in a Rayleigh fading environment," IEEE J. Sel. Areas Commun. **SAC-5**, 871–878 (1987).
19. P. W. Wolniansky, G. J. Foschini, G. D. Golden, and R. A. Valenzuela, "V-BLAST: An architecture for realizing very high date rates over the rich-scattering wireless channel," in *Proceedings of the URSI International Symposium on Signals, Systems, and Electronics* (IEEE, 1998), pp. 295–300.
20. R. van Nee, A. van Zelst, and G. Awater, "Maximum likelihood decoding in a space division multiplexing system," in *Proceedings of the 2000 IEEE, 51st Vehicular Technology Conference* (IEEE, 2000), Vol. 1, pp. 6–10.
21. W. Shieh, "Maximum-likelihood phase estimation for coherent optical OFDM," presented at the European Conference on Optical Communication, Berlin, Germany, 16–20 September 2007, paper Tu 4.2.2.

22. I. Barhumi, G. Leus, and M. Moonen, "Optimal training design for MIMO OFDM systems in mobile wireless channels," IEEE Trans. Signal Process. **41**, 1615–1624 (2003).
23. T. Pollet, M. van Bladel, and M. Moeneclaey, "BER sensitivity of OFDM systems to carrier frequency offset and Wiener phase noise," IEEE Trans. Commun. **43**, 191–193 (1995).
24. A. J. Lowery, L. B. Du, and J. Armstrong, "Orthogonal frequency division multiplexing for adaptive dispersion compensation in long haul WDM systems," in *Proceedings of the Optical Fiber Communication Conference* (IEEE, 2006), paper PDP 39.
25. R. Hui, B. Zhu, R. Huang, C. T. Allen, K. R. Demarest, and D. Richards, "Subcarrier multiplexing for high-speed optical transmission," J. Lightwave Technol. **20**, 417–427 (2002).
26. S. L. Jansen, I. Morita, and H. Tanaka, "10-Gb/s OFDM with conventional DFB lasers," presented at the European Conference on Optical Communication, Berlin, Germany, 16–20 September 2007, paper Tu. 2.5.2.